Int. J. Heat Mass Transfer. Vol. 33, No. 5, pp. 835–845, 1990
Printed in Great Britain

0017–9310/90 $3.00 + 0.00

Flow observations and mass transfer characteristics in symmetrical wavy-walled channels at moderate Reynolds numbers for steady flow

TATSUO NISHIMURA
Department of Chemical Engineering, Toyama University, Toyama 930, Japan

and

SHINICHIRO MURAKAMI, SHINGHO ARAKAWA and YUJI KAWAMURA
Department of Chemical Engineering, Hiroshima University, Higashi-Hiroshima 724, Japan

(*Received* 18 *May* 1989)

Abstract—Flow patterns and mass transfer characteristics in symmetrical two-dimensional wavy-walled channels are investigated at moderate Reynolds numbers: 20–300. We consider two different wall shapes: sinusoidal wall and arc-shaped wall. Two wall shapes are quite different in the development from laminar to transitional flow. In particular, a new flow structure consisting of a regular three-dimensional flow is observed at a low Reynolds number for the arc-shaped wall. This phenomenon leads to an earlier transition of turbulence as compared with the sinusoidal wall. Mass transfer characteristics of wavy-walled channels differ from those of a straight-walled channel when flow separation occurs. The arc-shaped wall has a larger mass transfer rate than the sinusoidal wall because of an earlier transition of turbulence.

1. INTRODUCTION

THE SYMMETRICAL wavy-walled channel is one of several devices employed for enhancing the heat and mass transfer efficiency of industrial transport processes having high Peclet numbers. The present authors [1–3] previously investigated flow and mass transfer characteristics in a channel with sinusoidal wavy walls for turbulent flow and concluded that the channel utilized yields a good mass transfer enhancement as compared to the corresponding straight-walled channel owing to an unsteady vortex motion in the furrows in the wall.

When this kind of channel is employed for medical devices such as a membrane oxygenator and a kidney dialyzer for the purpose of enhancing the mass transfer rates, the flow through channels may become laminar due to low Reynolds numbers, i.e. high viscosity and a narrow channel. The studies of laminar flow are necessary.

There have been several reports related to this problem. Sobey [4] performed a numerical computation assuming two-dimensional flow to examine flow patterns for steady and oscillatory flow in a channel with sinusoidal wavy walls which is a model of the Oxford membrane oxygenator operated under large oscillations with a much smaller mean flow (see Bellhouse *et al.* [5]). Stephanoff *et al.* [6] qualitatively confirmed the computational results of Sobey by flow visualizations. Furthermore, Stephanoff [7] studied the transition to turbulent flow in the same channel for steady flow by hot film gauges. On the other hand, there is little information on mass transfer. Only Aggarwal and Talbot [8] measured mass transfer rates in a single cavity for steady flow as a simple model of the Oxford membrane oxygenator. However, the real shape of the wall of the Oxford membrane oxygenator is a series of semi-circular arcs. It appears that the difference of the wall shapes remarkably affects flow structures and mass transfer characteristics. This has not been considered previously.

The purpose of this study is to examine the relation between flow patterns and mass transfer characteristics in symmetrical wavy-walled channels for two different wall shapes from laminar to transitional flow for steady flow.

Although not directly related to the present work, there have been many studies of transport phenomena in grooved channels and corrugated channels for laminar flow [9–15]. Most of them have been performed by the computations and have not confirmed the validity of assumptions included in the computations, e.g. limitations of laminar flow.

2. EXPERIMENTAL APPARATUS AND PROCEDURE

We have observed steady flow and measured the mass transfer rate in a rectangular channel in a purpose-built rig. The apparatus is shown schematically in Fig. 1. Water was pumped through the channel with a centrifugal pump. The flow rate was determined with a rotameter, and the fluid temperature was kept constant by a heat exchanger.

The channel consisted of a pair of undulated plates,

NOMENCLATURE

A	area of mass transfer surface [m^2]	Re	Reynolds number, UH_{max}/ν [—]
a	wave amplitude of wavy wall [m]	Sc	Schmidt number, ν/D [—]
C_b	concentration of ferricyanide ion [mol m^{-3}]	Sh	Sherwood number, $i_d H_{max}/FC_b AD$ [—]
D	molecular diffusivity of ferricyanide ion [m^2 s^{-1}]	U	velocity based on H_{max}, $Q/(H_{max}W)$ [m s^{-1}]
F	Faraday constant [C mol^{-1}]	W	width of wavy wall [m].
H_{max}	maximum spacing between walls [m]	Greek symbols	
i_d	diffusional current [A]	λ	wavelength of wavy wall [m]
L	mass transfer length [m]	λ_v	length of unit cell [m]
Q	volumetric flow rate [m^3 s^{-1}]	ν	kinematic viscosity [m^2 s^{-1}].

which are the principal walls. Two different undulated plates were employed to study the effect of wall shapes on the flow patterns and mass transfer characteristics. One is a sinusoidal wavy plate, and the other is a plate forming a series of semi-circular arcs which represents a real boundary shape of the Oxford membrane oxygenator. Figure 2 shows the dimensions of the channels which have a scale of approximately seven times that given for the oxygenator. There are 14 furrows in the wall of the channels; each furrow is 14 mm long (λ), 3.5 mm deep ($2a$) and 80 mm wide (W). The maximum gap between the upper and lower walls H_{max} is 10 mm. The aspect ratio of the channel based on the maximum gap is 8 and two-dimensional flow could be observed apart from the side walls. The experiment was designed so as to allow for measurements in the range of Reynolds number $Re = UH_{max}/\nu$ that is of particular interest to medical devices, i.e. 10–500.

Flow visualizations were by means of the aluminum dust method and the dye injection method. Perfusion with a suspension of aluminum particles, about 40 μm in diameter, enabled us to observe path lines corresponding to streamlines within the whole field of the flow. Rhodamine B dye was also injected from the wall to visualize particularly the wall region of the

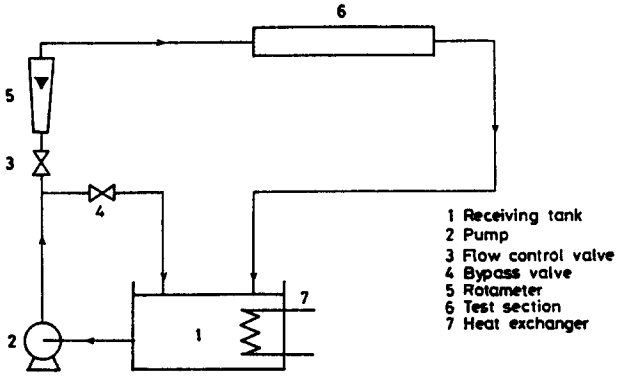

FIG. 1. Schematic diagram of experimental apparatus.

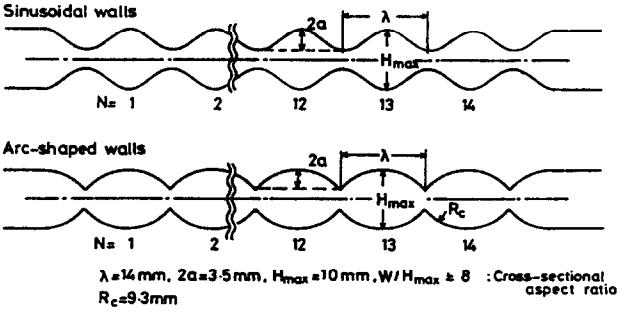

FIG. 2. Details of test section.

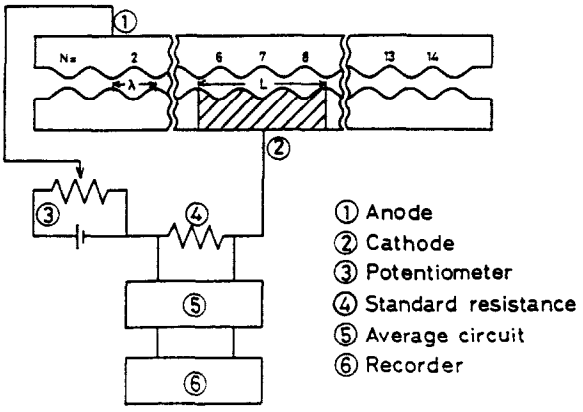

FIG. 3. Positions of electrodes and electrical circuit.

flow. Illumination was provided by a 500 W projector light source.

Since oxygen transport in blood by membrane oxygenators and urea removal by artificial kidneys belong to mass transfer with high Schmidt numbers, the mass transfer rates were obtained by measuring the diffusional current electrochemically (see, e.g. Mizushina [16]) to simulate transport of such substances from membrane surfaces to blood or vice versa. Three cathodes consisting of nickel-plated brass ($L/\lambda = 1, 2$ and 3) were used to determine the effect of the length of the mass transfer section on the average mass transfer rates. These cathodes were located from the sixth up to eighth wave sections in the lower wavy plate as shown in Fig. 3: the sixth wave section for $L/\lambda = 1$, the sixth and seventh wave sections for $L/\lambda = 2$ and the sixth to the eighth wave sections for $L/\lambda = 3$. The upper wavy plate, made of nickel-plated brass, was used for the anode. The electrolyte used contained 0.01 N potassium ferri–ferro cyanide and 1.0 N sodium hydroxide.

The Sherwood number Sh is related to the diffusional current i_d by

$$Sh = i_d H_{max}/FC_b AD.$$

The physical properties of the electrolyte presented by Mackley [17] were used in these experiments. The measurements were performed in the temperature range 15–30°C, which corresponds to the variation of Schmidt number ($Sc = 1231$–2636).

3. EXPERIMENTAL RESULTS AND DISCUSSION

3.1. *Flow pattern in channel with sinusoidal walls*

Figure 4 shows photographs of flow. An exposure time of 0.5 s was used. In the photographs the mainstream is moving from left to right and the location is from the sixth to the eighth wave sections in the channel. The flow is identical for each wave section, which confirms the fully developed flow. Figure 4(a) shows that at $Re = 20$ there is a considerable stagnant region in the upstream part of each furrow. It is difficult to determine whether separation has occurred because the particles move very slowly and are not displaced a great distance during the exposure time. At a Reynolds number of 50 (Fig. 4(b)) the recirculation vortex can be seen in the photograph and the vortices in the furrows have the same size in the upper and lower walls indicating a symmetric flow. On Fig. 4(c) the flow is shown at $Re = 100$. The vortex fills each furrow and the vortex center is located slightly downstream from the middle part of the furrow. As the Reynolds number increases further the vortex size hardly changes but the vortex center shifts to the downstream part of each furrow (Figs. 4(d) and (e)). Ultimately the flow becomes unsteady, i.e. shear layer oscillations, as the Reynolds number exceeds 300.

In an attempt to investigate the assumption of two-dimensional flow we observed the behavior of the accumulation of aluminum particles on the lower wall. The fluid motion was two-dimensional for most of the width of the channel in the range of Reynolds number considered here. A typical photograph is shown in Fig. 4(f) at $Re = 100$. The particles accumulate uniformly on the downstream part of each furrow where the flow is particularly slow.

The features shown in these photographs are consistent with two-dimensional numerical results of the previous study [1] as shown in Fig. 5, in particular the occurrence of separation near $Re = 20$ and the rapid growth of vortex to fill the furrow as the Reynolds number increases to near 100. The maximum value of the stream function within the vortex is shown in Fig. 6, which is obtained from the numerical computation. As the Reynolds number increases from 30 to 100 there is a rapid increase in the maximum stream function which corresponds to a rapid growth of the vortex size. These are similar to the results by Sobey [4], but the dimensions of the channel are slightly different, i.e. $2a/H_{max} = 0.35$ vs 0.33 and $\lambda/H_{max} = 1.4$ vs 1.33.

3.2. *Mass transfer in channel with sinusoidal walls*

The mass transfer rates at the sixth wave section for $L/\lambda = 1$ are presented in Fig. 7 as $Sh/Sc^{1/3}$ vs Re. Since

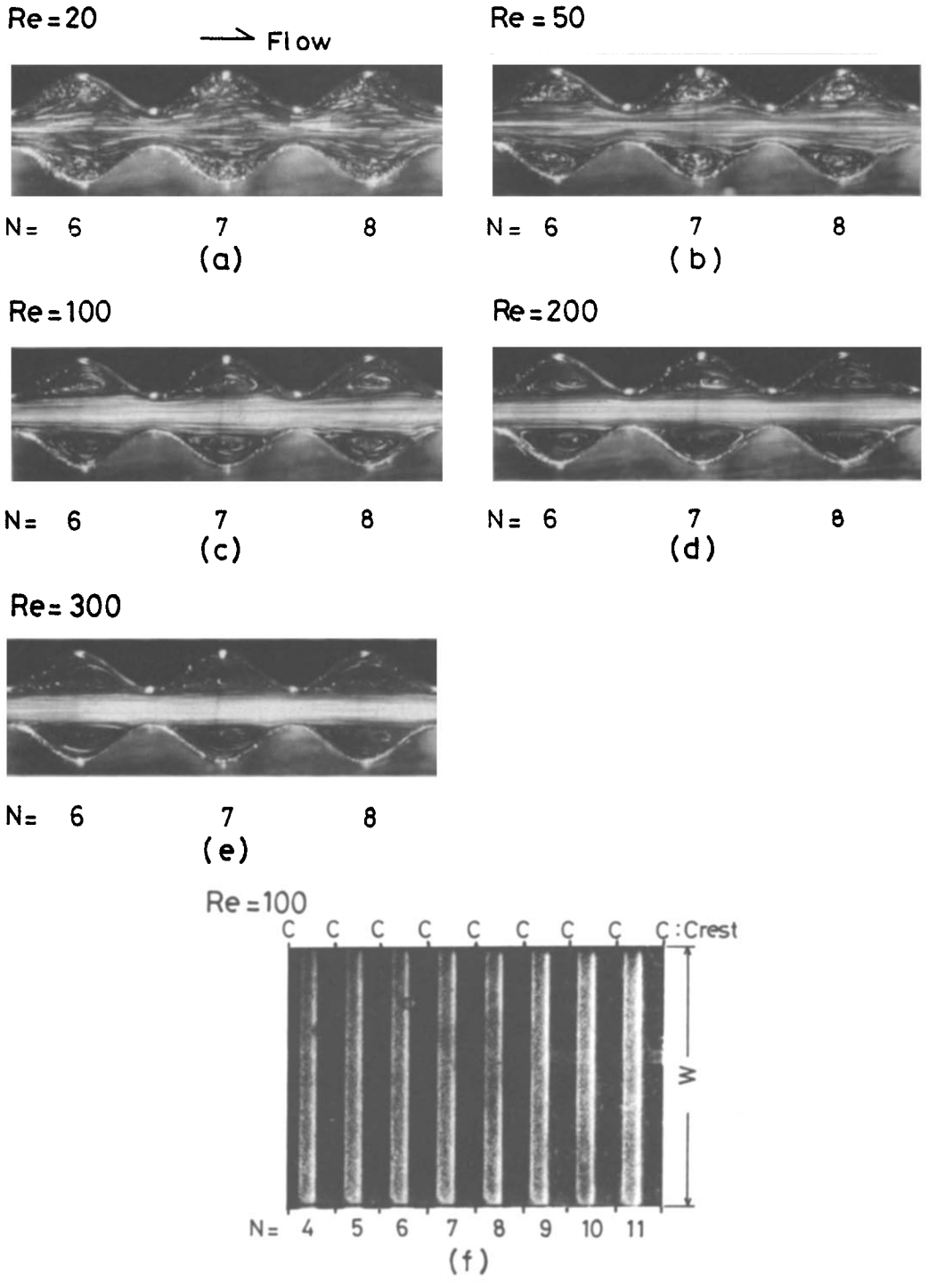

FIG. 4. Flow patterns for sinusoidal walls.

it is experimentally and theoretically well known that the Sherwood number is proportional to the 1 3 exponent of the Schmidt number for mass transfer of straight-walled channels with high Schmidt numbers, the data have been normalized with respect to $Sc^{1/3}$ to confirm the Schmidt number dependence for this channel. Three regions are clearly distinguished for the variation of the Sherwood number with the Reynolds number in this figure. We refer to these as Regions I, II and III. In particular the Sherwood numbers in Region II have a larger variation with the Reynolds number than those in Regions I and III, where there is a rapid growth of the vortex size and a rapid increase in the value of stream function within the vortex as mentioned above.

Figure 8 shows the effect of the mass transfer length. In Region I, the effect of the mass transfer length clearly appears and the Sherwood number is approxi-

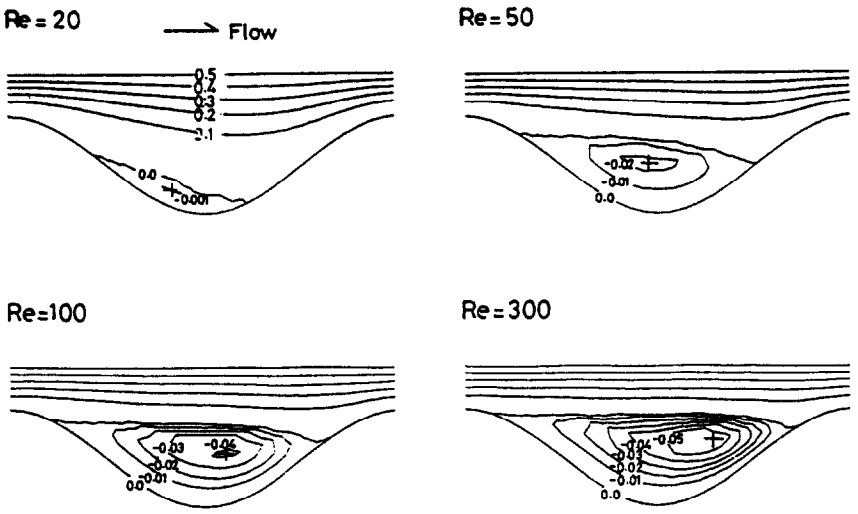

FIG. 5. Computed streamlines.

mately proportional to the $-1/3$ exponent of the mass transfer length, which is similar to that of the straight-walled channel obtained by Leveque theory also shown in this figure. Thus it is deduced that the effect of the flow separation is small in the initial stage of the recirculation vortex development and the concentration boundary layer is developed along the wavy surface (the sixth to eighth wave sections for $L/\lambda = 3$). In Region II, the effect of the mass transfer length becomes smaller as the Reynolds number increases. That is, the Reynolds number dependence increases for larger values of the mass transfer length. In Region III, the effect of the mass transfer length becomes insignificant. Thus the Sherwood number even for $L/\lambda = 1$ can be regarded as the fully developed value. The reason for this is considered to be that since the thickness of the concentration boundary layer for a system with high Schmidt number is very thin, the concentration boundary layer is cut off easily even by the steady recirculation vortex within each furrow of the channel and is periodically renewed from the reattachment point in each wavy section.

The present data connect well with the dotted line

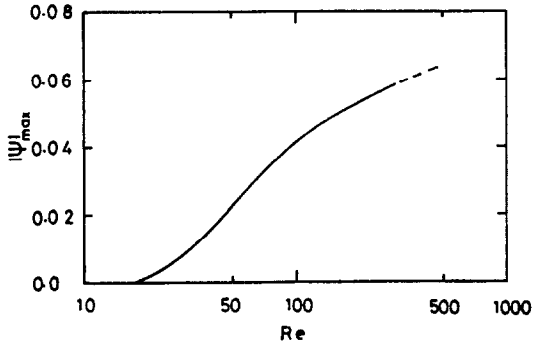

FIG. 6. Variation of stream function maximum in the recirculation vortex with Reynolds number.

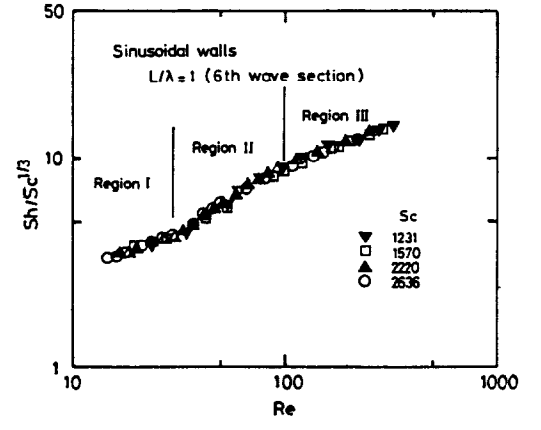

FIG. 7. Variation of Sherwood number with Reynolds number; effect of Schmidt number.

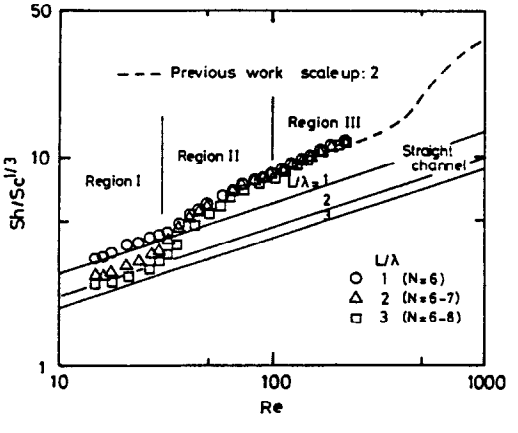

FIG. 8. Variation of Sherwood number with Reynolds number: effect of mass transfer length.

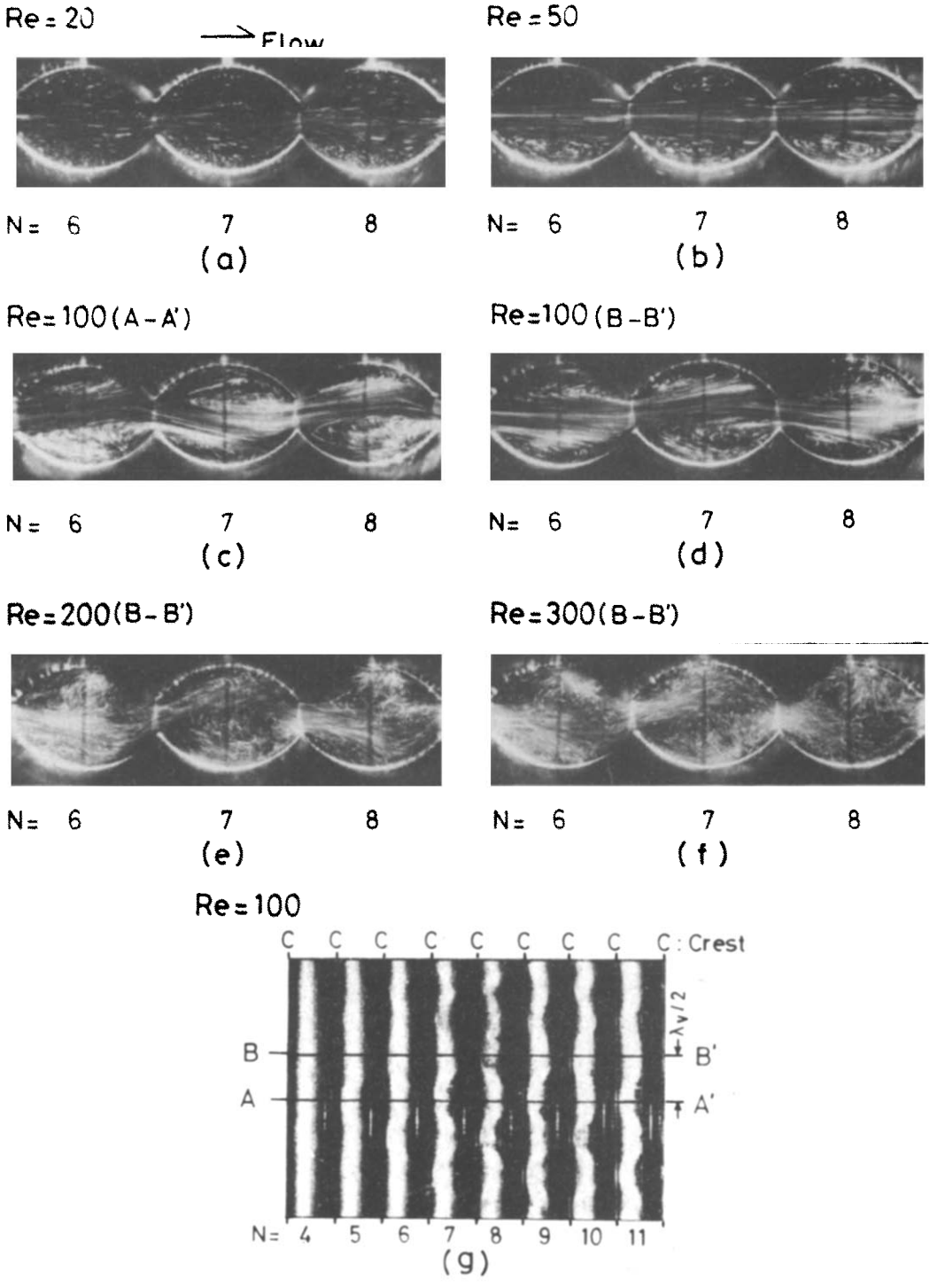

FIG. 9. Flow patterns for arc-shaped walls.

also shown in this figure which represents the result for turbulent flow in the wavy-walled channel having a scale of two times that given for the present study (see ref. [2]). A significant increment of the mass transfer rate at about $Re = 400$ is due to the transition to turbulent flow.

To examine the enhancement provided by the channel with wavy walls, the comparison of Sherwood number is performed between the wavy-walled channel and the straight-walled channel with the same gap as H_{max} in this figure under equal volumetric flow rate condition. The enhancement is scarcely expected in Region I, but becomes remarkable in Regions II and III. The trend is more significant with an increase in the mass transfer length. This is effective for the enhancement device.

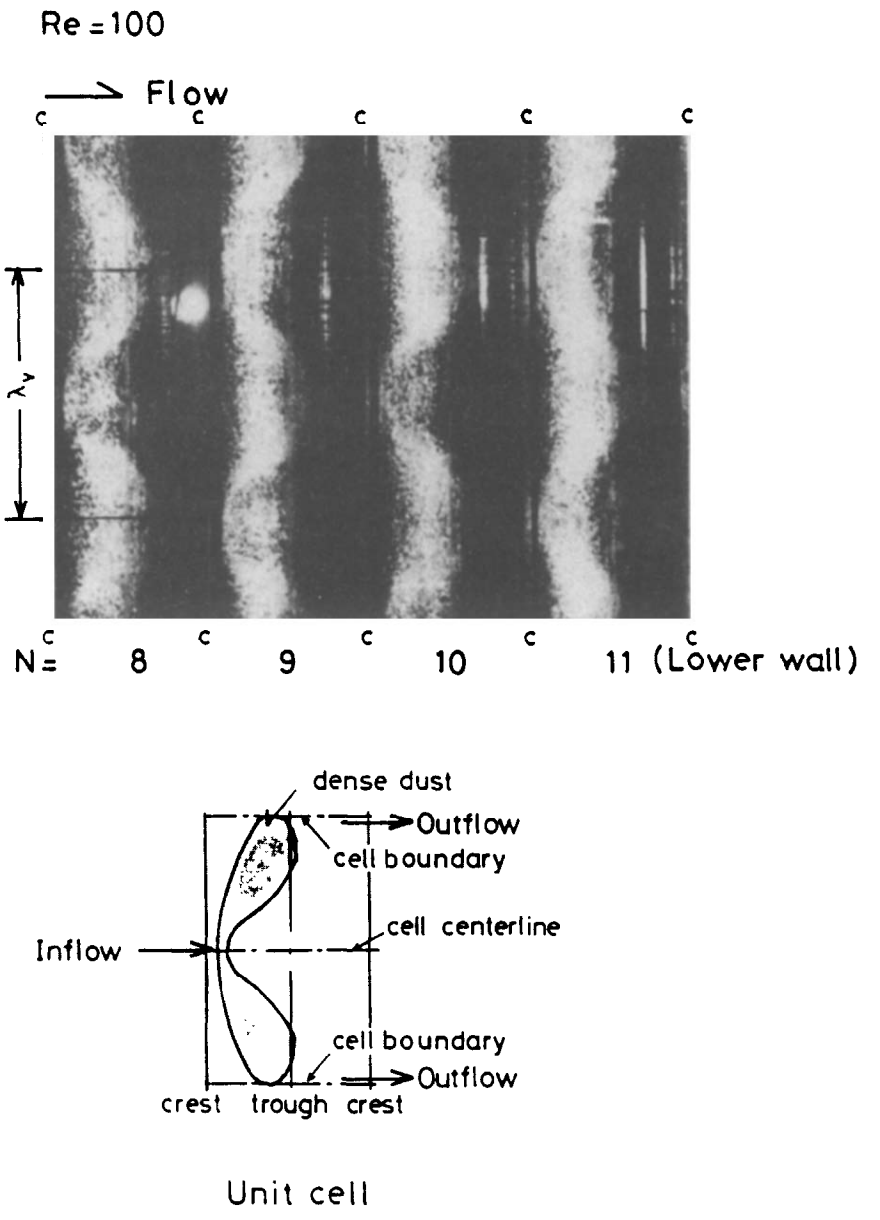

FIG. 10. Patterns of accumulation of aluminum particles on the lower wall.

3.3. *Flow pattern and mass transfer in a channel with arc-shaped walls*

Since this channel has a sharp edge at the crest in contrast to the case of a channel with sinusoidal walls, the nature of the separation will be affected by the sharpness and if so, the mass transfer of the channel will also be affected. Recently Greiner *et al.* [18] have identified that the critical Reynolds number for the onset of shear layer oscillations is very low in the case of an asymmetrically cusped wall channel.

Figure 9 shows photographs of the flow. At a small Reynolds number (Fig. 9(a)) there is a stagnant region in the upstream part of each furrow. As the Reynolds number increases the recirculation vortex is clearly observed. At $Re = 50$ (Fig. 9(b)), the separation point is located near the crest of the wall and the vortex size is slightly larger than that observed at the same Reynolds number in the case of sinusoidal walls (Fig. 4(b)). The main stream moves straight through the channel and thus the flow is symmetric at that stage.

An unexpected flow pattern is observed at $Re = 100$. The photograph of Fig. 9(g) represents the behavior of the accumulation of aluminum particles on the lower wall. In contrast to the case of sinusoidal walls (Fig. 4(f)), a periodical pattern with a constant wavelength λ_v is formed in the spanwise direction and also undergoes a 180° phase shift between adjacent furrows, which indicates three-dimensional flow with a regular structure. Figures 9(c) and (d) show the flows at two different longitudinal cross sections (A–A′ and B–B′) separated by a distance of a half wavelength $1/2\lambda_v$. From the comparison of both fig-

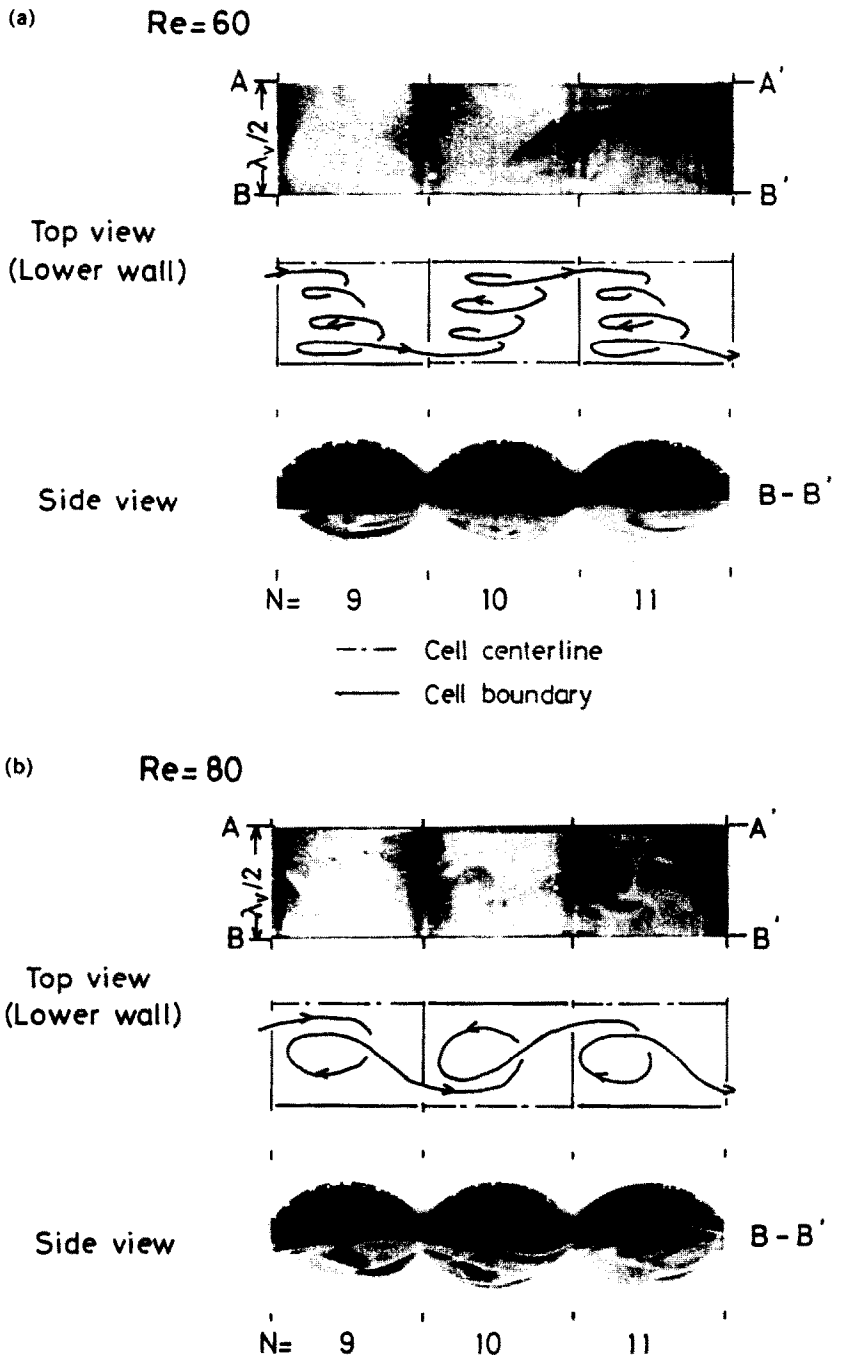

FIG. 11. Flow patterns within furrows: (a) $Re = 60$; (b) $Re = 80$.

ures, the main stream alternately deflects per one wave section through the channel, forming an asymmetric flow and also the deflection is reversed between the cross sections A–A′ and B–B′, but the flow behavior is identical. We focus on the flow within the furrows. At the lower furrows shown in Fig. 9(c), it seems as if the fluid springs from the upstream part of the sixth furrow, then enters the seventh furrow and is sucked into the upstream part. The eighth furrow has the same flow pattern as the sixth furrow. Thus the fluid in each furrow is not isolated but there is fluid communication among the furrows. The details are described later. As the Reynolds number exceeds 100 the flow becomes unsteady. Figures 9(e) and (f) show the results at the cross section B–B′ for $Re = 200$ and 300, respectively. Unsteady asymmetric flow develops and also turbulence exists. In the case of arc-shaped walls, the onset of turbulence occurs at a lower Reynolds number than in the case of sinusoidal walls.

We examine the structure of a new flow pattern observed in the present study. The behavior of the accumulation of aluminum particles on the lower wall is again shown in a magnified scale in Fig. 10. We call the region of one wavelength of λ_v 'a unit cell'. There

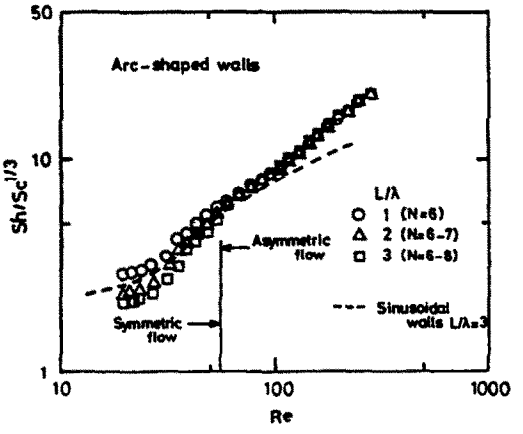

FIG. 12. Variation of Sherwood number with Reynolds number.

are dense parts near the cell boundaries and a sparse part in the cell centerline, as depicted in the schematic diagram. Contrasting Figs. 9(c), (d) and (g), the fluid in the upstream furrow enters the aimed furrow from the cell centerline, while the fluid in the aimed furrow jumps over the crest near the cell boundary and enters the downstream furrow. Thus the fluid in each furrow enters at the cell centerline and leaves at the cell boundary, i.e. inflow–outflow process, which leads to a regular three-dimensional structure. Some aspects of the pattern are still not clear, however. For instance, the question of fluid communication between inflow and outflow within each unit cell is not answered. The streakline of dye in furrows is observed to answer the question. Figure 11 shows some results. As the Reynolds number exceeds $Re = 55$, the main stream slightly deflects, i.e. transition of symmetric to asymmetric flow. As shown in the photograph at $Re = 60$ of Fig. 11(a), the dye streak moves with swirling from the cell centerline toward the cell boundary. Namely the vortex axis is not straight in the spanwise direction but is distorted having a transverse wave, which leads to the onset of the inflow–outflow process. A further increase of Reynolds number significantly changes the flow structure but the width of the unit cell λ, is constant as shown in Fig. 11(b). The dye streak forms a large loop between the cell centerline and the cell boundary. It is evident that the fluid within the unit cell exhibits a pair of tornado-like motions the axis of which is normal to the wall. The tornado-like motion causes a dense area of aluminum particles as shown in Fig. 10.

There is no clear guide to the existence of the regular three-dimensional flow. One possible cause of the effect is an instability of the purely two-dimensional motion to a perturbation of the separated shear layer position between the main stream and the recirculation vortex. In the case of arc-shaped walls, a sharp edge at the crest causes an asymmetric flow in spite of the symmetric channel as mentioned above. This phenomenon is known as the Coanda effect and there are similar observations in other flow fields, e.g. a two-dimensional symmetrical expanded channel. Although physical reasons for the occurrence of the asymmetric flow are not completely provided in the previous reports, Cherdron *et al.* [19] suggest that the origin of the asymmetry is related to eddy-like structures within the shear layers. Recently Sobey and Drazin [20] found by numerical calculation of flow in a two-dimensional symmetric indented channel that the Coanda effect is shown as a break in the symmetry of flow following a pitchfork bifurcation.

When the flow becomes asymmetric in wave sections for the arc-shaped wall system, the fluid leaves the furrow at the station where the separated shear layer is deflected upward. Continuity implies that the fluid has to enter the same furrow at the other station, where the separated shear layer is deflected downward. Such an explanation would show that the regular three-dimensional flow could exist. A similar observation has been reported for a single cavity in turbulent boundary layer flows by Maul and East [21] and Kistler and Tan [22], but it is not evident whether the reason for the three-dimensional flow is identical.

Figure 12 shows the results of mass transfer. As a whole, the mass transfer characteristics are similar to those for sinusoidal walls, i.e. the effect of the mass transfer length becomes small with increasing Reynolds number. The dotted line also shown in this figure indicates the case of sinusoidal walls at $L/\lambda = 3$. At Reynolds numbers less than 55 which represents the boundary between symmetric and asymmetric flows, arc-shaped walls have a smaller Sherwood number than sinusoidal walls. However, the tendency is reversed as the Reynolds number exceeds 55. This is due to the onset of turbulence following the three-dimensional flow as mentioned above.

4. CONCLUSIONS

We examined the relation between flow patterns and mass transfer characteristics in the symmetrical wavy-walled channels for two different wall shapes at moderate Reynolds numbers. The main results are as follows.

(1) The wavy-walled channels are characterized by flow separation within each furrow. At low Reynolds numbers the flow is kept two-dimensional for both sinusoidal and arc-shaped walls. However, as the Reynolds number increases, the wall shapes affect the flow structures. In particular for arc-shaped walls, a regular three-dimensional flow is generated due to asymmetric flow at a Reynolds number before the flow becomes unsteady. This phenomenon leads to an earlier transition of turbulence as compared with sinusoidal walls.

(2) Flow separation reduces the effect of the mass transfer length for both of the wall shapes, which implies a renewal of the concentration boundary layer

for a mass transfer system considered here. This yields mass transfer enhancement for laminar flow, but the degree of enhancement is smaller than that for turbulent flow. The mass transfer rates strongly depend on the strength of flow separation and the type of flow transition, and thus the difference in wall shapes affects the mass transfer rates.

Although wavy-walled channels with large cross-sectional aspect ratios would normally be considered to have two-dimensional flow, there is a possibility that an unexpected flow pattern such as a regular three-dimensional flow is generated by a wall shape. Thus the experimental study, as well as the computational study, is needed to know accurate flow patterns even at low Reynolds numbers.

REFERENCES

1. T. Nishimura, Y. Ohori and Y. Kawamura, Flow characteristics in a channel with symmetric wavy wall for steady flow, *J. Chem. Engng Japan* **17**, 466–471 (1984).
2. T. Nishimura, Y. Ohori, Y. Kajimoto and Y. Kawamura, Mass transfer characteristics in a channel with symmetric wavy wall for steady flow, *J. Chem. Engng Japan* **18**, 550–555 (1985).
3. T. Nishimura, Y. Kajimoto and Y. Kawamura, Mass transfer enhancement in channels with a wavy wall, *J. Chem. Engng Japan* **19**, 142–144 (1986).
4. I. J. Sobey, On flow through furrowed channels. Part 1. Calculated flow patterns, *J. Fluid Mech.* **96**, 1–26 (1980).
5. B. J. Bellhouse, F. H. Bellhouse, C. M. Curl, T. I. MacMillan, A. J. Gunning, E. H. Spratt, S. B. MacMurrung and J. M. Nelems, A high efficiency membrane oxygenator and pulsatile pumping system, and its application to animal trials, *Trans. Am. Soc. Artif. Int. Organs* **19**, 72–78 (1973).
6. K. D. Stephanoff, I. J. Sobey and B. J. Bellhouse, On flow through furrowed channels. Part 2. Observed flow patterns, *J. Fluid Mech.* **96**, 27–32 (1980).
7. K. D. Stephanoff, Self-excited shear-layer oscillations in a multi-cavity channel with a steady mean velocity, *Trans. ASME, J. Fluids Engng* **108**, 338–342 (1986).
8. J. K. Aggarwal and L. Talbot, Electro-chemical measurements of mass transfer in semi-cylindrical hollows, *Int. J. Heat Mass Transfer* **22**, 61–75 (1979).
9. I. S. Kang and H. N. Chang, The effect of turbulence promoters on mass transfer—numerical analysis and flow visualization, *Int. J. Heat Mass Transfer* **25**, 1167–1181 (1982).
10. D. H. Kim, I. H. Kim and H. N. Chang, Experimental study of mass transfer around a turbulence promoter by the limiting current method, *Int. J. Heat Mass Transfer* **26**, 1007–1016 (1983).
11. E. M. Sparrow and A. T. Prata, Numerical solutions for laminar flow and heat transfer in a periodically converging–diverging tube, with experimental confirmation, *Numer. Heat Transfer* **6**, 441–461 (1983).
12. R. S. Amano, A numerical study of laminar and turbulent heat transfer in a periodically corrugated wall channel, *Trans. ASME, J. Heat Transfer* **107**, 564–569 (1985).
13. M. Faghri and Y. Asako, Numerical determination of heat transfer and pressure drop characteristics for a converging–diverging flow channel, *Trans. ASME, J. Heat Transfer* **109**, 606–612 (1987).
14. Y. Asako and M. Faghri, Finite-volume solutions for laminar flow and heat transfer in a corrugated duct, *Trans. ASME, J. Heat Transfer* **109**, 627–634 (1987).
15. Y. Asako, H. Nakamura and M. Faghri, Heat transfer and pressure drop characteristics in a corrugated duct with rounded corners, *Int. J. Heat Mass Transfer* **31**, 1237–1245 (1988).
16. T. Mizushina, The electrochemical method in transport phenomena. In *Advances in Heat Transfer* (Edited by T. P. Irvine, Jr. and J. P. Hartnett), Vol. 7, pp. 87–161. Academic Press, New York (1971).
17. N. V. Mackley, Ph.D. Thesis, University of Aston in Birmingham (1973).
18. M. Greiner, G. E. Karniadakis, B. B. Mikic and A. T. Patera, Heat transfer augmentation and hydrodynamic stability theory: understanding and exploitation. In *Heat Transfer Korea—U.S. Seminar on Thermal Engineering and High Technology* (Edited by J. H. Kim, S. T. Ro and T. S. Lee), pp. 31–50. Hemisphere, Washington, DC (1988).
19. W. Cherdron, F. Durst and J. H. Whitelaw, Asymmetric flows and instabilities in symmetric ducts with sudden expansions, *J. Fluid Mech.* **84**, 13–31 (1978).
20. I. J. Sobey and P. G. Drazin, Bifurcations of two-dimensional channel flows, *J. Fluid Mech.* **171**, 263–287 (1986).
21. D. J. Maul and L. F. East, Three-dimensional flow in cavities, *J. Fluid Mech.* **16**, 620–632 (1963).
22. A. L. Kistler and F. C. Tan, Some properties of turbulent separated flows, *Physics Fluids* S165–S173 (1967).

OBSERVATION DES CARACTERISTIQUES DE L'ECOULEMENT ET DU TRANSFERT THERMIQUE DANS DES CANAUX SYMETRIQUES A PAROI ONDULEE POUR DES ECOULEMENTS PERMANENTS A NOMBRE DE REYNOLDS MODERE

Résumé—On étudie, pour des nombres de Reynolds modérés, les configurations d'écoulement et les caractéristiques de transfert thermique dans des canaux bidimensionnels à parois symétriques ondulées. On considère deux formes différentes de paroi : sinusoïdale et arquée. Elles sont très différentes vis-à-vis du passage de l'écoulement laminaire à la transition. En particulier, une nouvelle configuration d'écoulement consistant en un écoulement tridimensionnel régulier est observé pour un nombre de Reynolds faible avec la paroi arquée. Ce phénomène conduit à une transition à la turbulence anticipée en comparaison avec la paroi sinusoïdale. Les caractéristiques de transfert de masse pour les canaux à parois ondulées diffèrent de celles pour les canaux à parois planes lorsque se produit la séparation d'écoulement. La paroi arquée a un plus grand transfert que la paroi sinusoïdale à cause de la transition à la turbulence anticipée.

STRÖMUNGSFORM UND STOFFÜBERGANG IN KANÄLEN MIT SYMMETRISCH GEWELLTEN SEITENWÄNDEN BEI STATIONÄRER STRÖMUNG FÜR MITTLERE REYNOLDS-ZAHLEN

Zusammenfassung—Strömungsform und Stoffübergang in Kanälen mit zweidimensional symmetrisch gewellten Seitenwänden werden für mittlere Reynolds-Zahlen (20–300) untersucht. Zwei verschiedene Wandprofile (kreisbogenförmig und sinusförmig) werden betrachtet, bei denen die Entwicklung von laminarer zur Übergangsströmung ziemlich unterschiedlich ist. Im besonderen wird bei kleinen Reynolds-Zahlen bei der bogenförmig ausgebildeten Wand eine neue Strömungsform beobachtet, die eine dreidimensionale regelmäßige Strömung aufweist. Der Übergang zur Turbulenz findet hier früher statt als bei der sinusförmig ausgebildeten Wand. Der Stoffübergang in Kanälen mit gewellten Wänden unterscheidet sich von dem in Kanälen mit geraden Wänden—sobald Strömungsablösung eintritt. Die bogenförmig ausgebildete Wand führt wegen des früheren Übergangs zur Turbulenz zu einem besseren Stoffübergang als die sinusförmig ausgebildete Wand.

ИССЛЕДОВАНИЕ ПОТОКОВ И ХАРАКТЕРИСТИК МАССОПЕРЕНОСА В СИММЕТРИЧНЫХ КАНАЛАХ С ВОЛНИСТЫМИ СТЕНКАМИ ПРИ УМЕРЕННЫХ ЧИСЛАХ РЕЙНОЛЬДСА В СЛУЧАЕ УСТАНОВИВШЕГОСЯ ТЕЧЕНИЯ

Аннотация—Исследуются картины течения и характеристики массопереноса в симметричных двумерных каналах с волнистыми стенками при умеренных значениях числа Рейнольдса, изменяющихся в диапазоне 20–300. Рассматриваются две различные формы стенок: синусоидальная и дугообразная. Обе формы различно влияют на развитие течения от ламинарного к переходному. В частности, в случае дугообразной стенки при низких значениях числа Рейнольдса наблюдается новая структура, представляющая собой правильное трехмерное течение. Это приводит к более ранней турбулизации потока, чем в случае синусоидальной стенки. Характеристики массопереноса в каналах с волнистыми стенками отличаются от характеристик, полученных при отрыве течения в канале с прямыми стенками. В случае дугообразной стенки массоперенос более интенсивен, чем в случае синусоидальной формы, что объясняется более ранней турбулизацией потока.